Advanced modeling of NiTi stents used in minimally invasive surgeries

Msc. Sharath Chavalla [1)], Jun.-Prof. Dr.-Ing. Daniel Juhre [2)]

[1)] Institut of Mechanics, Otto von Guericke University Magdeburg, Germany, sharath.chavalla@ovgu.de

[2)] Institute of Mechanics, Otto von Guericke University Magdeburg, Germany, daniel.juhre@ovgu.de

Abstract

Computation modelling based on the finite element method (FEM) has proven to be an important tool to gain insights into the mechanical performance of structures and hence very popular. Inspite of a popular computation tool, FEM has its own drawbacks. The geometry of the structures is in most cases approximated using linear polynomial functions resulting in a compromise of geometrical accuracy. In such cases, geometrical accuracy can only be improved by increasing the number of elements. This increases the computation effort of the problem. In recent years, a numerical method has been developed which can significantly bridge the gap between computer aided design (CAD) and FEM. This method is called isogeometric analysis (IGA) which is based on representation and calculation of geometries using non-uniform rational B-splines (NURBS). Unlike FEM, IGA uses high-order and high-regular basis functions. This yields in improving the accuracy of the results with a minimal computation effort. The aim of current study is to contribute to the efficient bending simulation of the deformation behavior of carotid NiTi stents in throat arteries using IGA which can lead to a step closer in realizing real-time simulation of stents.

Keywords: stents, NiTi alloy

1. Introduction

Cardiovascular diseases are one of the main reasons of death in western countries. In such diseases, arteries develop a plaque resulting in narrowing (stenosis) and hence reducing the blood flow through them. Stenosis leads to stroke which often occur without prior warning. Although many treatment procedures exist, future trend seems to progress towards treatment involving percutaneous minimally invasive surgery techniques. In such operating procedures, high-tech implants are deployed along an endoluminal path into the pathological area. One such family of implants are called as stents, which are characterized by their complex geometries and unique material properties. For effective use of stents in surgeries, continuous technological improvements regarding the material, design and operating conditions are inevitable. Treatment procedures optimized for individual patients (predictive medicine) is gaining importance these days and such treatment is not possible without using robust and cost-effective simulation methods.

With regards to deployment of stents in the arteries, they are classified into balloon-expandable and self-expandable. Since their introduction in markets self-expandable stents have become a primary choice for today's stenting procedures. Self-expandable stents are made of Nickel Titanium (NiTi) alloys which are also known as shape memory alloys (SMA). In addition to the shape memory effect these alloys exhibit pseudoelasticity which makes their choice highly favorable. The pseudoelastic effect exhibited by NiTi is a result of diffusionless transformation of the microstructure of the material from martensite to austenite phase and this helps in maintaining the flexibility (strains of 10% can be recovered) of the stent structure.

The complexity of stent implant as a result of its material property, geometry and loading conditions makes it difficult to effectively characterize its mechanical behavior. Also proper stent deployment plays an important role in successful intervention procedure. Stent flexibility is evaluated by performing bending on stents and are of greater significance in the stent delivery process. Hence qualitative evaluation of mechanical properties and influence of geometry design on the performance of stent is necessary. Finite element analysis (FEA) is a popular tool to perform such evaluations in order to test different configurations before prototype testing. Inspite of being a popular tool FEA poses problems in terms of approximating the geometry and accuracy of the approximated solution. The low-order and low-regularity polynomials used in discretization of continuum domain do not capture the exact geometry unless highly fine meshes are used.

Isogeometric analysis (IGA) is a recently developed computation tool which bridges the gap between computer aided design (CAD) and computation analysis. IGA replaces low-order, low regular FEA basis functions with high-order, high-regular basis functions used in CAD and retaining isoparametric framework. Non-uniform rational B-splines (NURBS) were initially chosen as basic environment for IGA due to their extensive use in CAD community [1].

In the current study the bending behavior of stents is analyzed using classical FEA and IGA in a finite deformation regime. This is based on cantilever beam bending test proposed by Müller-Hülsbeck et al.,[2]. The paper is structured as follows: in section 2 a brief overview of non uniform rational B-splines (NURBS) and the IGA concept is given. In the following section the computation procedure to develop IGA suitable stent geometry from CAD geometry including brief description of the constitutive material model used for the analysis setup is detailed. In section 4 the numerical results are presented and analyzed comparing reaction force per different degrees of freedom pertaining to different refinements of FEA and IGA models.

2. Basics of NURBS and IGA

In this section a brief outlook on trivariate NURBS is given. For further information please refer to the work of Hughes.et.al.,[3]. NURBS are constructed from B-splines which are expressed as piecewise polynomials and are widely used in CAD and computer graphics. A pth order B-spline $\mathbf{C}(\xi)$ is obtained by a combination of B-spline basis functions and coefficients $\mathbf{B}_i$ defined in real space and are named as control points as follows:

$$\mathbf{C}(\xi) = \sum_{i=1}^{n} N_{i,p}(\xi)\mathbf{B}_i \tag{2.1}$$

n is the total number of basis functions and control points. The parameter space of the curve is described by a variable ξ. A knot vector Ξ is defined as a non-decreasing vector with real values.

$$\Xi = [\xi_1, \xi_2, \xi_3, ...\xi_{n+p+1}] \tag{2.2}$$

The knots ξ_i partition the parameter space into knot spans. Given a knot vector Ξ B-spline basis functions are recursively defined as

$$N_{i,0}(\xi) = \begin{cases} 1 & if \quad \xi_i < \xi < \xi_{i+1} \\ 0 & otherwise \end{cases} \tag{2.3}$$

$$N_{i,p}(\xi) = \frac{\xi - \xi_i}{\xi_{i+p} - \xi_i} N_{i,p-1}(\xi) + \frac{\xi_{i+p+1} - \xi}{\xi_{i+p+1} - \xi_{i+1}} N_{i+,p-1}(\xi) \tag{2.4}$$

A pth order NURBS curve is defined as

$$\mathbf{C}(\xi) = \sum_{i=1}^{n} R_{i,p}(\xi)\mathbf{B}_i \text{ ,with } \quad R_{i,p}(\xi) = \frac{N_{i,p}(\xi)w_i}{\sum_{i=0}^{n} N_{i,p}(\xi)w_i} \tag{2.5}$$

where w_i are the projection weights and $N_{i,p}$ are pth order B-spline basis functions. NURBS curves retain all the properties of B-spline curves like high continuity and regularity. Equation (2.5) can be extended to solids as follows

$$\mathbf{V}(\xi_1, \xi_2, \xi_3)_d = \sum_{i=0}^{n_1} \sum_{j=0}^{n_2} \sum_{k=0}^{n_3} R_{i,p}(\xi_1) S_{j,q}(\xi_2) T_{k,r}(\xi_3) (\mathbf{B}_{i,j,k})_d \tag{2.6}$$

where $(\mathbf{B}_{i,j,k})_d$ are coordinates of control points, *p,q,r* are polynomial degrees and $R_{i,p}, S_{j,q}, T_{k,r}$ are the NURBS basis functions in each parametric direction respectively. The described NURBS basis functions are then introduced as a galerkin isoparametric method based on those shape functions in IGA.[1]

3. Material model and Geometry

In this section the procedure to construct the stent models compatible with IGA framework directly from CAD is decribed. An overview of the constitutive material model is described. The stent geometry and the material model are then used with in analysis setup to simulate stent bending test.

3.1. Stent Model

The procedure involving generation of CAD model and integrating with general purpose solver FEAP is explained. The geometry is generated using software ‚Rhinoceros Version 5 SR14 64-bit' and an example model of a stent is constructed. The type of stent structure considered for the present study is a ‚closed-cell' stent in which all the junctions in the stent are connected with each other.

The stent geometry suitable for IGA is created in RHINO in the following steps.

1. Initially a 2D surface pattern of desired stent design is drawn on a base surface as shown in Fig 3.1.

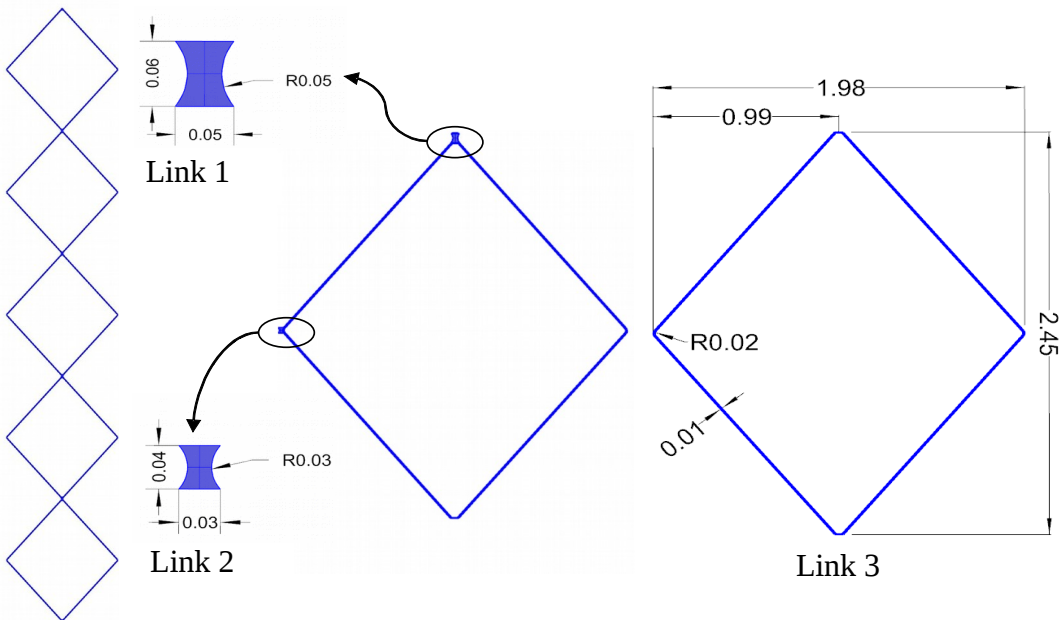

Fig 3.1: 2D Surface patch details of the stent design

2. A cylindrical surface is constructed whose diameter is equal to the inner diameter of the stent structure.

3. The 2D surface pattern is then wrapped around the cylinder of inner radius 2.0 mm to obtain the stent strucuture.

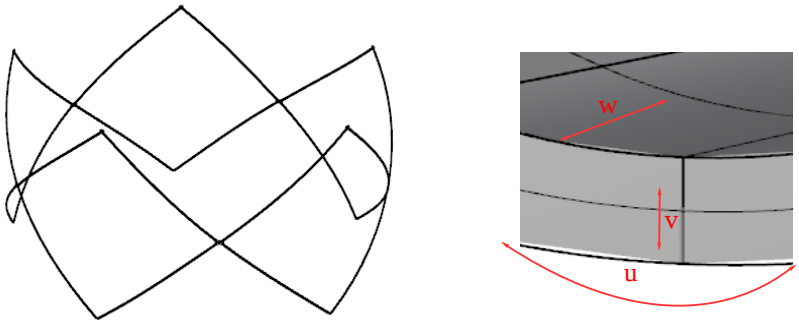

Fig 3.2: NURBS patch model for IGA with detailed view of three parametric directions u,v and w

Each 2D CAD surface generates a NURBS patch. The above steps generate a single row of stent geometry which is shown in Fig 3.2, this single row needs to be further extended. The NURBS data for all the patches is then exported as text files using GEO PDEs plugin [4]. The exported text files (containing NURBS data for a single row of stent) are then used to generate the extruded geometry and FEAP compatible input file using in-house Matlab codes.

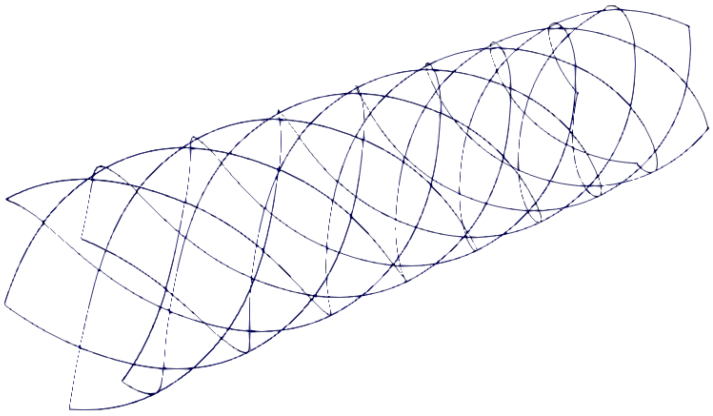

Fig 3.3: Extended IGA-stent model

The extended stent model (see Fig 3.3) comprised of 400 patches. The basic stent structure is composed of three different link patches namely link 1, link 2 and link 3 as shown in Fig 3.1. Initially, the link patches 2 and 3 are quartic-linear-quadratic elements in circumferential (u), longitudinal (v) and thickness (w) directions, where as for link 1 the patch is quartic-linear-linear. The IGA polynomial order are obtained from 2D NURBS patch for circumferential and longitudinal directions, the thickness polynomial order is quadratic. For further refinements of the IGA patch, the knot insertion is done for link 3 (see Fig 3.1). The number of subdivisions varied from 1 to 8 for knot insertion for the NURBS model.

The equivalent finite element meshes are generated directly from the NUBRS model. It should be noted that as the order of NURBS model is quartic in circumferential direction, this leads to a refined FE mesh at the stent curvature. The finest NURBS model is used for creating finite element mesh using in-house routines. The FE mesh is further refined (h-refinement) using non uniform subdivision of each patch. For FEA mesh trilinear brick elements with full integration are used.

The knot insertion is acheived using in-house matlab code and FEA refinement is accomplished through codes which are implemented as add-on in FEAP. The following tables: Table 3.1 and Table 3.2 represent the IGA and FEA files after the respective refinements.

FEA:

Mesh Name	DOF	Degree	Number of subdivisions		
			u	v	w
FEA551	242,100	linear	5	5	1
FEA661	339,570	linear	6	6	1
FEA771	453,360	linear	7	7	1
FEA881	583,470	linear	8	8	1
FEA1081	733,770	linear	10	8	1
FEA1281	878,790	linear	12	8	1
FEA1381	953,940	linear	13	8	1
FEA1482	1,539,675	linear	14	8	2
FEA2082	2,196,225	linear	20	8	2
FEA3082	3,295,755	linear	30	8	2
FEA4082	4,387,365	linear	40	8	2

Table 3.1: List of FEA models after h-refinement

IGA:

Mesh Name	DOF	Order		
		Link 1 (u,v,w)	Link 2 (u,v,w)	Link 3 (u,v,w)
IGA0	41,400	4,4,2	4,1,2	4,1,2
IGA2	44,280	4,4,2	4,1,2	4,1,2
IGA3	47,160	4,4,2	4,1,2	4,1,2
IGA4	50,040	4,4,2	4,1,2	4,1,2
IGA7	58,680	4,4,2	4,1,2	4,1,2

Table 3.2: List of IGA models after knot insertion

3.2. Constitutive material model

In order to capture the behavior of self-expanding NiTi stents, the phenomenological model proposed by Christ.et.al., [5] in the context of finite deformations is adopted. The elastic deformation gradient $\mathbf{F}_e$ is defined by the relation

$$\mathbf{F}_e := \mathbf{F}\mathbf{F}_t^{-1} \Longrightarrow \mathbf{F} = \mathbf{F}_e\mathbf{F}_t \tag{2.1}$$

The phase transformation in polycrystalline shape memory alloys does not proceed steadily due to the presence of internal dislocations. This phenomena is described by the elastic part $\mathbf{F}_{t_e}$ of the transformation deformation.

$$\mathbf{F}_{te} := \mathbf{F}_t\mathbf{F}_{td}^{-1} \Longrightarrow \mathbf{F}_t = \mathbf{F}_{te}\mathbf{F}_{td} \tag{2.2}$$

The Green-Lagrange strain tensor is defined as $\mathbf{E} = (\mathbf{C} - \mathbf{1})/2$, where $\mathbf{C} = \mathbf{F}_t\mathbf{F}$ is the right Cauchy-Green tensor. The transitional strain tensor is defined as $\mathbf{E}_t = (\mathbf{C}_t - \mathbf{1})/2 = (\mathbf{F}_t^T\mathbf{F}_t - \mathbf{1})/2$, additionally elastic right Cauchy-Green tensor $\mathbf{C}_e$ is used.

$$\mathbf{C}_e = {\mathbf{F}_e}^T\mathbf{F}_e = \mathbf{F}_t^{-T}\mathbf{C}\mathbf{F}_t^{-1} \tag{2.3}$$

and its transitional part

$$\mathbf{C}_{t_e} = \mathbf{F}_{t_e}^T\mathbf{F}_{t_e} = \mathbf{F}_{t_d}^{-T}\mathbf{C}_t\mathbf{F}_{t_d}^{-1} \tag{2.4}$$

The complete material law can be summarised as follows:

- Stress quantities

$$\mathbf{S} = 2\mathbf{F}_t^{-1}\frac{\partial\psi_e}{\partial\mathbf{C}_e}\mathbf{F}_t^{-T} \tag{2.5}$$

$$\mathbf{X} = \mathbf{X}_t + \mathbf{X}_z \tag{2.6}$$

$$\mathbf{X}_t = \mathbf{F}_{t_d}^{-1}2\frac{\partial\psi_t}{\partial\mathbf{C}_{t_e}}\mathbf{F}_{t_d}^{-T},\ \mathbf{X}_z = \frac{\Delta\psi}{\beta}\frac{\mathbf{E}_t}{||\mathbf{E}_t||} \tag{2.7}$$

$$\mathbf{Y} = \mathbf{C}\mathbf{S} - \mathbf{C}_t\mathbf{X} \text{ and } \mathbf{Y}_t = \mathbf{C}_t\mathbf{X}_t \tag{2.8}$$

- Evolution equations: $\dot{\mathbf{C}_t} = 2\dot{\lambda}\frac{1}{||\mathbf{Y}^D||}(\mathbf{Y}^D\mathbf{C}_t),\ \dot{\mathbf{C}_{t_d}} = 2\dot{\lambda}\frac{b}{\mu_t}(\mathbf{Y}_t^D\mathbf{C}_{t_d})$ (2.9)

- Kuhn-Tucker conditions: $\dot{\lambda} \geq 0,\ \ \phi_{SMA} \leq 0,\ \dot{\lambda}.\phi_{SMA} = 0$ (2.10)

where $\phi_{SMA} = \left\|\mathbf{M}^D - \mathbf{X}^D\right\| - k,\ \mathbf{M} := 2\mathbf{C}_e \dfrac{\partial \Psi_e}{\partial \mathbf{C}_e}$, k is the half height of hysteresis curve and Ψ_e represents elastic part of Helmholtz free energy function. The superscript D indicates the deviatoric part of the respective measure.

- Martensitic volume fraction: $z = \dfrac{||\mathbf{E}_t||}{\beta},\ 0 \leq z \leq 1$ (2.11)

The constitutive material parameters are obtained from Christ.et.al., [5] which were fit to experimental tests of Helm and Haupt [6,7].

3.3. Analysis Setup

The problem that is being considered in the current context is bending of a stent. Bending test is performed considering the proposal by Auricchio.et.al., [1,8]. The stent is clamped at one end and displacement boundary conditions are applied to the control points as shown in the Fig 3.4 at the free end.

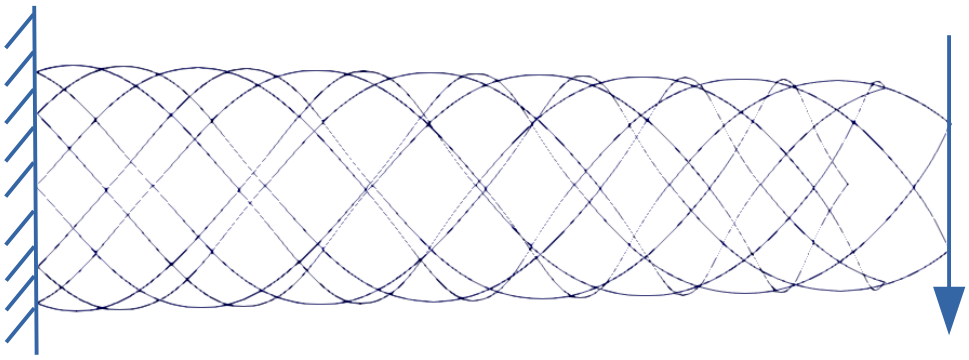

Fig 3.4: Boundary conditions on the stent

The displacement of u = 8.5 mm is applied for simulating the bending behavior of the stent. The resultant of reaction forces at the free end is considered as a reference measure to compare the ability of IGA and FEA to efficiently simulate stent bending. The FEA and IGA analysis are performed for the refined meshes as explained in section 3.2.

4. Results and Discussion

In the current section the results of the stent bending simulation with respect to the different refinements of FEA and IGA models are explained.

Initially the convergence of all the IGA and FEA models with respect to the reaction force at the free end against number of degrees of freedom of the stent are analysed as shown in the Fig. 4.1.

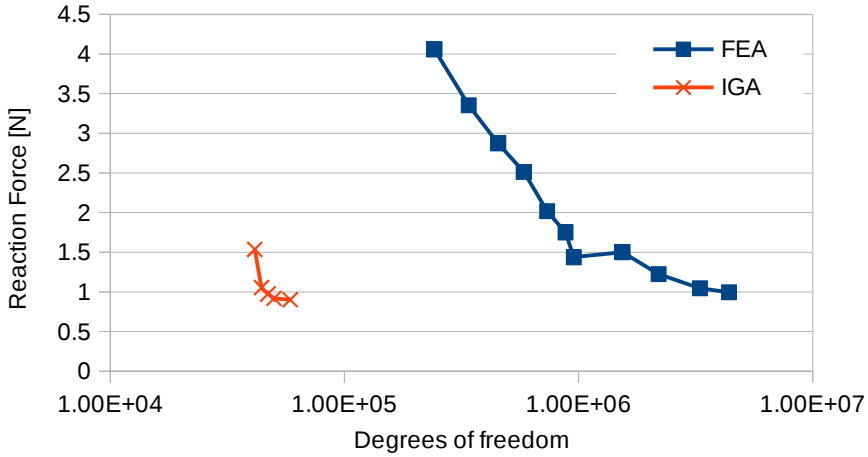

Fig. 4.1: Reaction force convergence plots

The force-displacement curves for all the iterations of FEA and IGA are shown in Fig 4.2. In Fig 4.3 a comparison is made between the results of finest, coarsest IGA models against the finest FEA model.

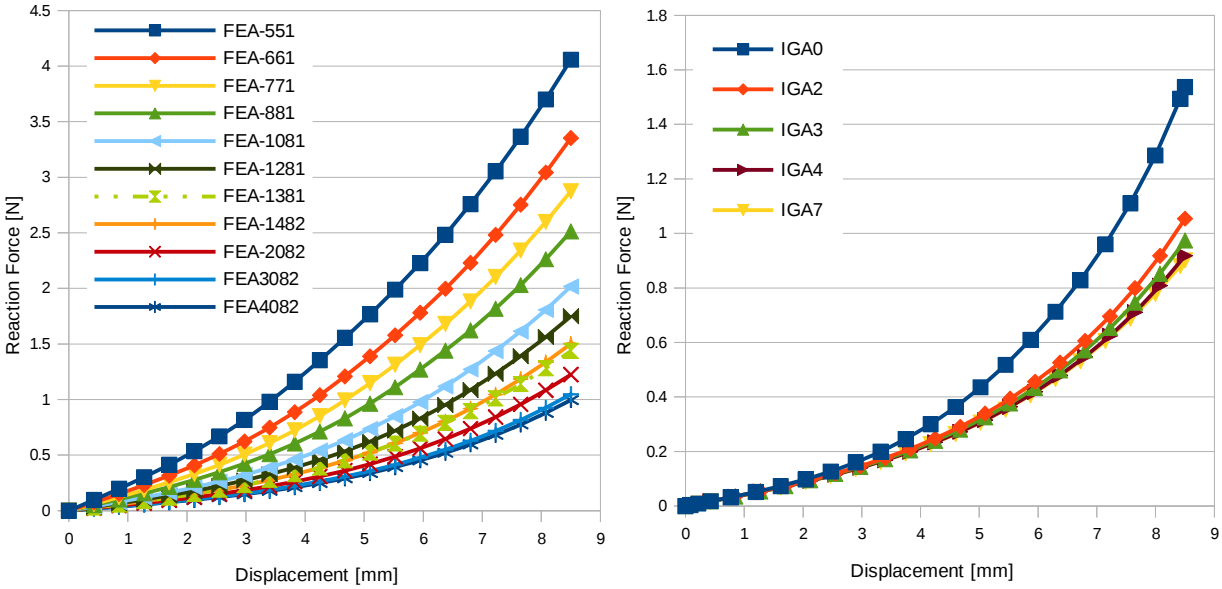

Fig. 4.2: Reaction force - Displacement curves for FEA and IGA models

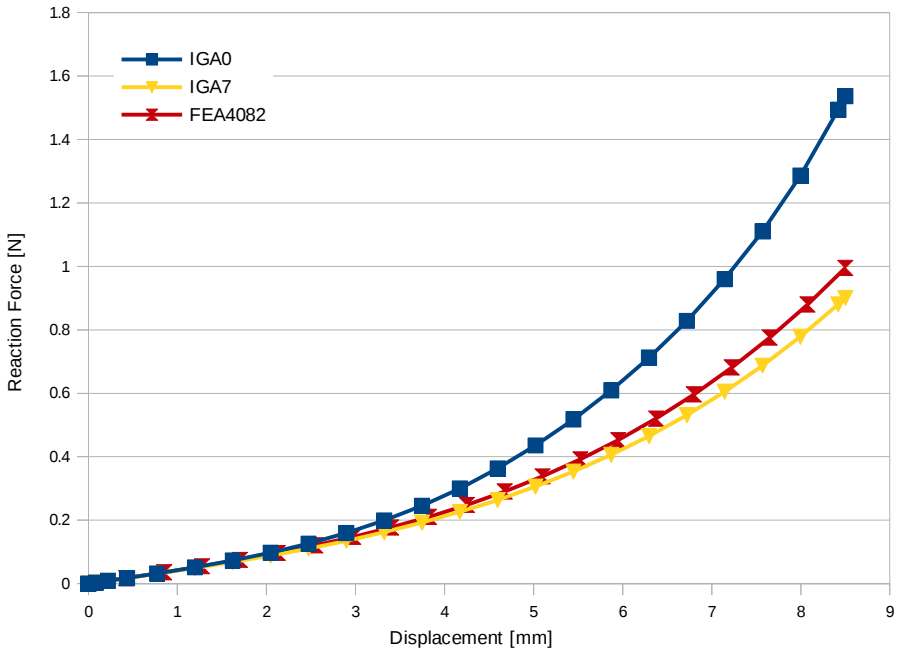

Fig.4.3: Reaction force - Displacement curves for finest FEA vs coarsest and finest IGA models

All the results concerning reaction force and degrees of freedom pertaining to all the models are presented in Table 4.1.

Mesh name	DOF	Reaction Force	
		Measure [N]	% Error
FEA551	242,100	4.0580	77.80
FEA661	339,570	3.3520	73.14
FEA771	453,360	2.8739	68.66
FEA881	583,470	2.5131	64.16
FEA1081	733,770	2.0174	55.35
FEA1281	878,790	1.7496	48.52
FEA1381	953,940	1.4379	37.36
FEA1482	1,539,675	1.5015	40.01
FEA2082	2,196,225	1.2243	26.43
FEA3082	3,295,755	1.0468	13.95
FEA4082	4,387,365	0.9953	9.50
IGA0	41,400	1.5367	41.38
IGA2	44,280	1.0540	14.54
IGA3	47,160	0.9739	7.52
IGA4	50,040	0.9179	1.88
IGA7	58,680	0.9007	0

Table 4.1: Reaction forces – Stent bending

The percentage error shown in Table 4.1 is calculated for all the iterations of stent model in comparison with the finest IGA model, i.e., IGA7. The advantage of IGA in predicting the reaction force values against FEA with relatively lower degrees of freedom of orders less than a factor of 10 is to be noted. This trend can also be graphically observed in Fig 4.1. Also IGA models converge faster than the FEA with repect to the number of refinements. The finest FEA model with degrees of freedom 4,387,365 has a relative error of 9.50% with respect to finest IGA model whose degrees of freedom are only 58,680. This is clearly observed in Fig 4.3 that high refinement of FEA model is required so that the predicted reaction force value lies with in the range of values predicted by IGA method.

Similarly when force-displacement curves (see Fig 4.2) are analysed, it can be observed that the trend for both the cases is similar.

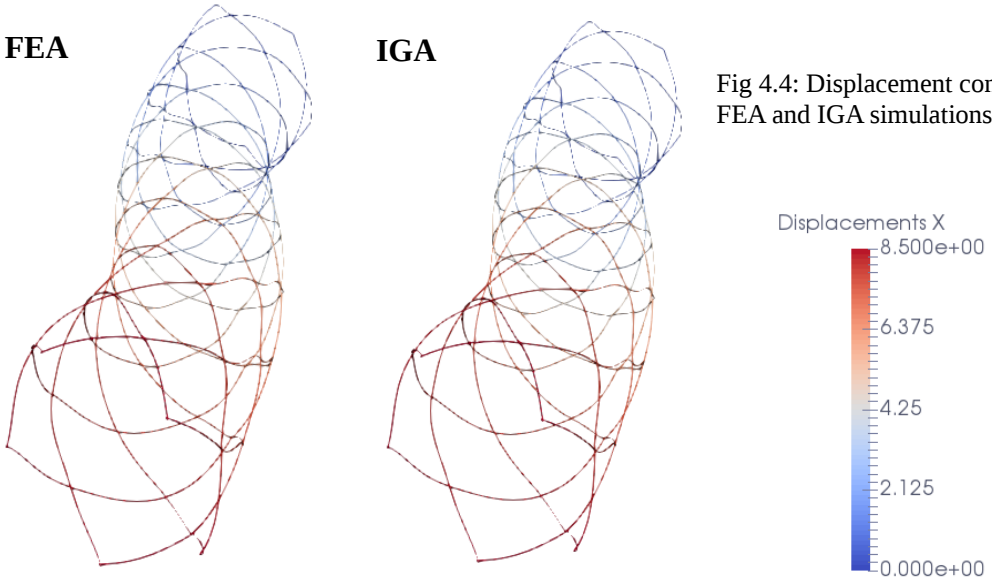

Fig 4.4: Displacement contour plot for FEA and IGA simulations

The deformed configurations of the stent for the respective fine mesh models is depicted in Fig 4.4. In this figure it can be observed that IGA and FEA yield similar deformed configurations. The potential of IGA to simulate bending behavior of stent in comparison to FEA simulation in terms of performance with respect to degrees of freedom is noteworthy.

It is to be mentioned that reaction force is a measure that represents local behavior unlike global quantity like deformation energy. Auricchio.et.al [1] compared the reaction force results with deformation energy results and concluded that both the quantities follow similar convergence trends. Hence the choice of reaction force as a performance indicator for stent bending analysis is justified.

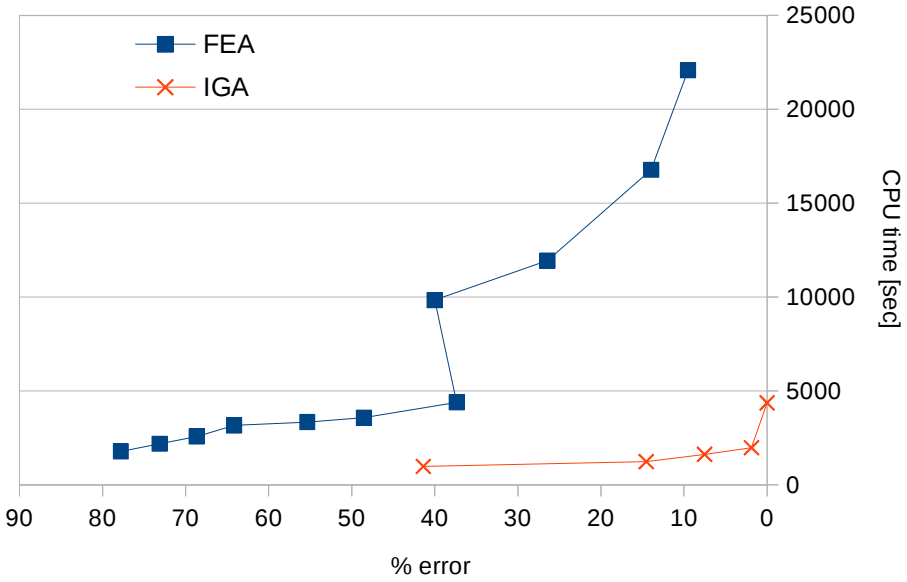

Fig 4.5: CPU time vs %error: FEA and IGA

The % error mentioned in Table 4.1 is compared with the CPU time to analyse computational time between both the methods. This is shown in the Fig 4.5.

The graph clearly shows that IGA is computationally less expensive. As an example considering a relative error of around 14%, FEA3082 consumed 16779 seconds against IGA2 with 1238 seconds of CPU time. In addition to this, when finest IGA and FEA models are compared, IGA is approximately 5 times faster that FEA. However futher comparisons of FEA and IGA are necessary in terms of different approximation degrees for FEA and integration rules for IGA.

4. Conclusion

In the current study the computational methodology for integrating CAD models with IGA is presented. The computation domain is accurately represented in IGA unlike requirement of extremely fine mesh in the case of FEA. This study demonstrates the superiority of IGA to produce numerical results better than the traditional FEA with relatively low number of degrees of freedom and lesser computation times. In future work the potential of IGA in realising contact between the stent and artery is planned along with fluid-structure simulations to simulate blood flow through the artery with stent.

Acknowledgments

This work is partly funded by the Federal Ministry of Education and Research within the Forschungscampus STIMULATE under grant number 13GW0095A and by the European Regional Development Fund under the operation number ‚ZS/2016/04/78123‘ as part of the initiative „Sachsen-Anhalt WISSENSCHAFT Schwerpunkte“.

References

[1] Auricchio, F.; Conti, M.; Ferraro, M.; Morganti, S.; Reali, A.; Taylor, R.L.: Innovative and efficient stent flexibility simulations based on isogeometric analysis. Computer methods in Applied Mechanics and Engineering 295, (2015) 347-361

[2] Müller-Hülsbeck, S.; Schafer, P.; Charalambous, N.; Schaffner, S.; Heller, M.; Jahnke, T.: Comparison of carotid stents: an in-vitro experiment focusing on stent design, J. Endovasc. Ther. 16 (2009) 168–177

[3] Hughes, T.; Cottrell, J.; Bazilevs, Y.: Isogeometric analysis: Cad, finite elements, nurbs, exact geometry, and mesh refinement, Comput. Methods Appl. Mech. Engrg. 194 (2005) 4135–4195

[4] De Falco, C.; Reali, A.; Vázquez, R.: Geopdes: A research tool for isogeometric analysis of pdes, Adv. Eng. Softw. 42 (2010) 1020–1034

[5] Daniel, C.; Reese, S.: Finite deformation pseudo-elasticity of shape memory alloys – Constitutive modelling and finite element implementation, International Journal of Plasticity 24, (2008) 455-482

[6] Helm, D.; Haupt, P.; Thermomechanical behaviour of shape memory alloys. Active Materials: Behavior and Mechanics 4333, (2001) 302–313

[7] Helm, D.; Haupt, P.: Shape memory behaviour: modelling within continuum mechanics. International Journal of Solids and Structures 40, (2003) 827–849

[8] Auricchio, F.; Arghavani, J.; Conti, M.; Morganti, S.; Reali, A.; Stefanelli, U.: Shape-memory, alloys: effective 3D modeling, computational aspects and analysis of actuator and biomedical devices. Proceedings of ACTUATOR10 - International Conference and Exhibition on New Actuators and Drive Systems., 2010